Bar-driven evolution and quenching of spiral galaxies in cosmological simulations

Spinoso, Daniele ; Bonoli, Silvia ; Dotti, Massimo ; Mayer, Lucio ; Madau, Piero ; Bellovary, Jillian

Abstract: We analyse the outputs of the cosmological 'zoom-in' hydrodynamical simulation ErisBH to study a strong stellar bar which naturally emerges in the late evolution of the simulated Milky Way-type galaxy. We focus on the analysis of the formation and evolution of the bar and on its effects on the galactic structure, the gas distribution and the star formation. A large central region in the ErisBH disc becomes bar unstable after z 1.4, but a clear bar starts to grow significantly only after z 0.4, possibly triggered by the interaction with a massive satellite. At z 0.1, the bar stabilizes and reaches its maximum radial extent of l 2.2 kpc. As the bar grows, it becomes prone to buckling instability. The actual buckling event, observable at z 0.1, results in the formation of a boxy-peanut bulge clearly discernible at z = 0. During its early growth, the bar exerts a strong torque on the gas and drives gas inflows that enhance the nuclear star formation on sub-kpc scales. Later on, as the bar reaches its maximum length and strength, the gas within its extent is nearly all consumed into stars, leaving behind a gas-depleted region in the central 2 kpc. Observations would more likely identify a prominent, large-scale bar at the stage when the galactic central region has already been gas depleted, giving a hint at the fact that bar-driven quenching may play an important role in the evolution of disc-dominated galaxies.

DOI: https://doi.org/10.1093/mnras/stw2934

Originally published at:
Spinoso, Daniele; Bonoli, Silvia; Dotti, Massimo; Mayer, Lucio; Madau, Piero; Bellovary, Jillian (2016). Bar-driven evolution and quenching of spiral galaxies in cosmological simulations. Monthly Notices of the Royal Astronomical Society, 465(3):3729-3740.
DOI: https://doi.org/10.1093/mnras/stw2934

Monthly Notices of the ROYAL ASTRONOMICAL SOCIETY

MNRAS **465,** 3729–3740 (2017) doi:10.1093/mnras/stw2934
Advance Access publication 2016 November 17

Bar-driven evolution and quenching of spiral galaxies in cosmological simulations

Daniele Spinoso,[1,2★] Silvia Bonoli,[2] Massimo Dotti,[1,3] Lucio Mayer,[4,5] Piero Madau[6] and Jillian Bellovary[7]

[1] *Università degli Studi di Milano-Bicocca, Piazza della Scienza 3, I-20126 Milano, Italy*
[2] *Centro de estudios de fisí ca del cosmos de Aragó n, plaza San Juan, 1 planta-2 E-44001 Teruel, Spain*
[3] *INFN, Sezione di Milano-Bicocca, Piazza della Scienza 3, I-20126 Milano, Italy*
[4] *Center for Theoretical Astrophysics and Cosmology, Institute for Computational Science, University of Zurich, Winterthurerstrasse 190, CH-8057 Zäurich, Switzerland*
[5] *Kavli Institute for Theoretical Physics, Kohn Hall, University of California, Santa Barbara, CA 93106-4030, USA*
[6] *Department of Astronomy and Astrophysics, University of California, 1156 High Street, Santa Cruz, CA 95064, USA*
[7] *Department of Astrophysics, American Museum of Natural History, Central Park West and 79th St, New York, NY 10024, USA*

Accepted 2016 November 9. Received 2016 November 9; in original form 2016 July 7

ABSTRACT

We analyse the outputs of the cosmological 'zoom-in' hydrodynamical simulation ErisBH to study a strong stellar bar which naturally emerges in the late evolution of the simulated Milky Way-type galaxy. We focus on the analysis of the formation and evolution of the bar and on its effects on the galactic structure, the gas distribution and the star formation. A large central region in the ErisBH disc becomes bar unstable after $z \sim 1.4$, but a clear bar starts to grow significantly only after $z \simeq 0.4$, possibly triggered by the interaction with a massive satellite. At $z \simeq 0.1$, the bar stabilizes and reaches its maximum radial extent of $l \approx 2.2$ kpc. As the bar grows, it becomes prone to buckling instability. The actual buckling event, observable at $z \simeq 0.1$, results in the formation of a boxy-peanut bulge clearly discernible at $z = 0$. During its early growth, the bar exerts a strong torque on the gas and drives gas inflows that enhance the nuclear star formation on sub-kpc scales. Later on, as the bar reaches its maximum length and strength, the gas within its extent is nearly all consumed into stars, leaving behind a gas-depleted region in the central $\sim$2 kpc. Observations would more likely identify a prominent, large-scale bar at the stage when the galactic central region has already been gas depleted, giving a hint at the fact that bar-driven quenching may play an important role in the evolution of disc-dominated galaxies.

Key words: methods: numerical – galaxies: bulges – galaxies: evolution – galaxies: formation – galaxies: kinematics and dynamics – galaxies: structure.

1 INTRODUCTION

Bars are extremely common non-axisymmetric features in disc galaxies, occurring in up to $\gtrsim$30 per cent of massive ($M_* \gtrsim 10^{9.5}\,\mathrm{M}_\odot$) spirals in the local Universe (Laurikainen, Salo & Buta 2004; Nair & Abraham 2010; Lee et al. 2012a; Gavazzi et al. 2015b; Consolandi et al. 2016). Bars are considered to play a key role in the evolution of disc galaxies, being able to drive strong inflows of gas towards the central galactic regions (e.g. Sanders & Huntley 1976; Roberts, Huntley & van Albada 1979; Athanassoula 1992) and triggering nuclear starbursts (e.g. Ho, Filippenko & Sargent 1997; Martinet & Friedli 1997; Hunt & Malkan 1999; Laurikainen et al. 2004; Jogee, Scoville & Kenney 2005). Bars are also thought to be responsible for the build-up of the pseudo/discy bulges, whose nearly exponential profiles hints to a disc origin (e.g. Kormendy 2013, for a review). These structures are the most common type of bulges among galaxies in the stellar mass range $10^{9.5}\,\mathrm{M}_\odot < M_* < 10^{10.5}\,\mathrm{M}_\odot$, while classical bulges dominate among more massive systems (e.g. Fisher & Drory 2011). Bars can also be responsible for triggering AGN activity, if a fraction of the inflowing gas can reach the central sub-pc of the galaxy (e.g. Shlosman, Frank & Begelman 1989; Berentzen et al. 1998; Sellwood & Moore 1999; Combes 2001; Fanali et al. 2015; Querejeta et al. 2016).

On longer time-scales, the removal of the gas forced towards nuclear regions affects the star formation processes within the bar extent (Cheung et al. 2013; Fanali et al. 2015; Hakobyan et al. 2016),

★ E-mail: d.spinoso@campus.unimib.it

contributing to the lowering of the specific star formation rate in the most massive spiral galaxies at low redshift (Cheung et al. 2013; Gavazzi et al. 2015b). In addition to the effect of the bar on to the inter stellar medium (ISM), the dynamical evolution of the bar itself is advocated to be responsible for the boxy/peanut-shaped stellar bulges (B/P bulges hereafter; see Kormendy 2013; Sellwood 2014, for a review), observed in $\gtrsim$40 per cent of edge on disc galaxies (e.g. Lütticke, Dettman & Pohlan 2000). Together with the high fraction of discy pseudo-bulges, the frequent occurrence of B/P bulges hints at the fundamental importance of secular evolution in the shaping of the central regions of disc galaxies.

Most of the theoretical studies which support the existence of causal connections between bars and the above-mentioned structures/processes are either analytical or based on simulations of isolated galaxies (e.g. Athanassoula 1992; Berentzen et al. 1998; Regan & Teuben 2004; Berentzen et al. 2007; Villa-Vargas, Shlosman & Heller 2010; Kim, Seo & Kim 2012; Cole et al. 2014). Although these kind of simulations are extremely informing about the dynamical effect of bars, cosmological simulations are needed to follow bar formation within the hierarchical growth of galaxies (as discussed in, e.g. Kormendy 2013). Furthermore, most of the simulation literature on bar formation and evolution is based on collisionless simulations. Several works have employed hydrodynamics and star formation, showing interesting differences on important issues such as bar survival and bar buckling (see e.g. Athanassoula, Lambert & Dehnen 2005; Debattista et al. 2006; Athanassoula, Machado & Rodionov 2013; Gabor & Bournaud 2014; Thacker et al. 2014; Roos et al. 2015); however, none of them has employed modern sub-grid recipes for feedback in a cosmological context, which constitute a crucial aspect of recent progress in simulating galaxy formation.

To date, only a handful of fully cosmological simulations have achieved the required numerical resolution and included all the physical processes needed to self-consistently produce barred galaxies (e.g. Romano-Díaz et al. 2008; Kraljic, Bournaud & Martig 2012; Scannapieco & Athanassoula 2012; Goz et al. 2014; Fiacconi, Feldmann & Mayer 2015; Okamoto, Isoe & Habe 2015; Bonoli et al. 2016). Among the above-mentioned cosmological simulations of barred disc galaxies, ErisBH (Bonoli et al. 2016) and ARGO (Fiacconi et al. 2015) share the highest spatial and mass resolutions,[1] but ARGO has been evolved only down to $z = 3$, while ErisBH has been followed down to $z = 0$, so its properties can be compared directly with the observed properties of well-resolved barred galaxies.

ErisBH is a twin simulation of Eris (Guedes et al. 2011), with which it shares initial conditions, resolution and sub-grid physics, but, unlike Eris, it also includes prescriptions for the formation, growth and feedback of supermassive black holes. Both Eris and ErisBH resemble, at $z = 0$, a late-type galaxy such as the Milky Way, but while Eris hosts a typical pseudo-bulge, ErisBH features a strong bar and its bulge has a clear boxy-peanut morphology (Bonoli et al. 2016).

The aim of this work is to study the build-up and the evolution of the strong bar seen in Eris*BH,* to learn about the origin of bars and the impact that these structures have in shaping galaxies like our own Milky Way.

The paper is organized as follows. In Section 2, we briefly summarize the properties and main results of the ErisBH simulation. In Section 3, we study the build-up of the bar, quantifying its strength and radial extent; we analyse the dynamical properties of the galaxy disc, testing its stability to non-axisymmetric perturbations and looking for resonances between the bar bulk precession and the orbital motions of disc stars; we also analyse the formation of the B/P morphology of the bulge. In Section 4, we show the impact of the bar in depleting gas and triggering star formation in the central region of the galaxy. Finally, in Section 5 we summarize and discuss our results.

2 THE ErisBH SIMULATION

ErisBH (Bonoli et al. 2016) is one of the runs of the Eris-suite simulations (Guedes et al. 2011, 2013; Mayer 2012; Shen et al. 2012, 2013; Bird et al. 2013; Rashkov et al. 2013; Sokolowska et al. 2016) which have been among the first zoom-in cosmological simulations to produce realistic late-type spirals with properties comparable to those of the Milky Way at $z = 0$. ErisBH inherits its initial condition and most of its features from the first Eris run (Guedes et al. 2011, 2013), from which it differs in that it also includes prescriptions for the formation and accretion of massive black holes (MBHs) and their associated AGN feedback. Here, we summarize the main characteristics of the Eris simulation and the new sub-grid physics implemented in ErisBH . For more details, we refer the reader to Guedes et al. (2011) and Bonoli et al. (2016).

Eris was obtained from a zoom-in of a Milky Way-sized halo selected within a low-resolution, dark matter-only simulation of a (90Mpc)^3 volume. This simulation assumed a flat universe with $\Omega_{\rm M} = 0.24$, $\Omega_{\rm b} = 0.042$, $h_0 = 73\,{\rm km\,s^{-1}\,Mpc^{-1}}$, $n = 1$ and $\sigma_8 = 0.76$ obtained from the *WMAP* three-year data (Spergel et al. (2007)). The target halo was selected also because of its quiet merger history (i.e. no mergers with a mass ratio above 1:10 after $z = 3$), which allows us to primarily attribute the galaxy evolution to internal, dynamical processes rather than to strong external perturbations. Such a quiet merger history is not a common feature (only ∼10 per cent of Milky Way-sized haloes experienced their last major merger at $z \gtrsim 3$, see Fakhouri, Chung-Pei & Boylan-Kolchin 2010, and references therein) and is mainly due to the fact that Eris is a field disc galaxy belonging to a low-density environment. The cosmological evolution of the haloes was simulated from $z = 90$ down to $z = 0$ with the parallel *N*-body spatially and temporally adaptive tree-SPH code GASOLINE (Wadsley, Stadel & Quinn 2003).

Within the high-resolution region, the initial dark matter and gas particles masses were set, respectively, to $m_{\rm DM} = 9.8 \times 10^4\,{\rm M}_{\odot}$ and $m_{\rm g} = 2 \times 10^4\,{\rm M}_{\odot}$. The gravitational softening length was fixed to the value of $\varepsilon_0 = 120$ physical parsec for each particle type from $z = 0$ to 9 and evolved as $\varepsilon(z) = \varepsilon_0(1 + z)^{-1}$ from $z = 9$ to 90. ErisBH , as the original Eris, includes recipes for Compton and atomic cooling of hot primordial gas, heating from a UV background and metallicity-dependent radiative cooling at low ($<10^4$ K) gas temperatures (Guedes et al. 2011). Energy and metals injection in the ISM due to supernovae (SNe) explosions and stellar feedback are modelled following the recipe of Stinson et al. (2010).

Owing to the high resolution of the simulation, we could use a relatively high-density threshold for star formation, i.e. $n_{\rm SF} = 5$ atoms cm^{-3}. The combination of SNe feedback and the high-density threshold for star formation produces a realistic clumpy ISM (Guedes et al. 2011) and removes low angular momentum gas from the simulated disc. The final outcome of ErisBH is a Milky Way-sized disc galaxy with a low bulge-to-disc (B/D) ratio and a flat rotation curve (with rotation velocity at the solar radius of 190 $\pm$ 15 km s^{-1}), whose location on the Tully–Fisher, stellar mass/halo mass, and stellar velocity dispersion–MBH mass relations is

[1] The simulations by Kraljic et al. (2012) have a comparable spatial resolution but a coarser resolution in mass.

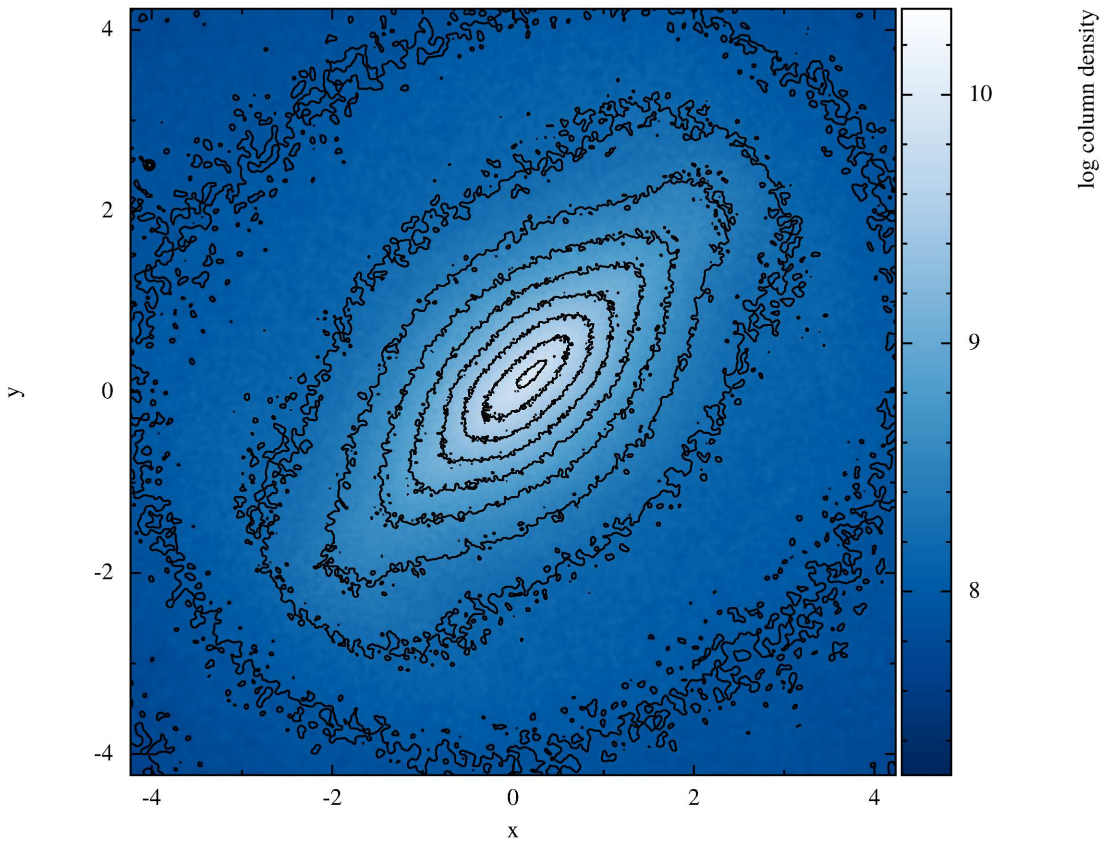

Figure 1. Stellar surface density Σ_* map of the central region of the ErisBH galaxy at redshift $z = 0$. The x- and y-axis units are in [kpc h^{-1}], while the colour shades show the values of $\log(\Sigma_*/\mathrm{M}_\odot\ \mathrm{kpc}^{-2})$. The black solid lines are the iso-density contours used to reveal the inner structure of the bar and to show that the non-axisymmetric shape is maintained even at very small radius. Contours are separated by a 0.2 difference in $\log(\Sigma_*)$ starting from a value of $\log(\Sigma_*/\mathrm{M}_\odot\ \mathrm{kpc}^{-2}) = 9.8$ in the centre. Note that the deviation from axisymmetry increases at smaller and smaller radii so that the central bar structure is more elongated than the global bar structure. This feature is common in all the snapshots where the bar is observable.

consistent with that of the Milky Way. Note that at $z > 0.5$ both ErisBH and Eris have overly efficient star formation relative to abundance-matching predictions, while they agree with it at $z = 0$. Recent runs in the Eris suite which incorporate both metal-line cooling and stronger SN feedback, do obey abundance-matching constraints at higher redshift but miss a kinematically cold thin disc component at $z = 0$ (Sokolowska et al. 2016).

ErisBH includes recipes for the seeding, growth and thermal feedback of MBHs. Growth occurs by both mergers with other MBHs and gas accretion. All the other parameters in this new run were kept identical to those in the original Eris in order to allow a coherent comparison between the two simulations. In ErisBH, an MBH seed is placed in every halo that (i) does not already host an MBH, (ii) is resolved with at least 10^5 particles and (iii) hosts at least 10 gas particles in regions denser than 100 atoms cm^{-3}. Only four protogalaxies in the simulation match the above-mentioned conditions before $z \sim 3$ and are thus seeded with an MBH, whose mass is proportional to the size of the high-density gas region. After $z \sim 3$, the gas density becomes generally too low for the seeding process to occur (Bonoli et al. 2016). The four black hole seeds are then allowed to accrete mass following the Bondy–Hoyle–Lyttleton prescription capped at the Eddington limit, as implemented in Bellovary et al. (2010). During the accretion phase, it is assumed that a small fraction $\epsilon_f = 0.05$ of the total AGN luminosity couples with the surrounding gas and heats it. The growth of the black hole hosted by the central galaxy is mostly due to mergers with black holes hosted by infalling satellite galaxies, while growth by gas accretion is very modest, as reflected by the low accretion rates measured, typically between 10^{-3} and 10^{-5} M$_\odot$ yr^{-1} (i.e. only 10^{-2}–10^{-4} of the Eddington limit; an exhaustive and extended discussion on the growth of the black holes in ErisBH can be found in Bonoli et al. 2016). Despite the limited gas growth, the modest feedback energy released by the central black hole still manages to affect the large-scale properties of the host galaxy. For example, ErisBH features a smaller bulge and a more extended disc when compared to Eris. Because of the absence of a prominent central mass concentration, the disc in ErisBH is prone to dynamical instabilities during late evolutionary stages (e.g. Kormendy 2013, and references therein) and a clear stellar bar develops within the central ∼3 kpc of the disc. A qualitative analysis of the stellar surface density field in late evolutionary stages of ErisBH can easily point out the presence of a central non-axisymmetric feature, i.e. a stellar bar (see the lower-left panel of fig. 10 in Bonoli et al. 2016, and Fig. 1 here for a zoom-in of the central galactic regions).

In the next sections, we focus on studying the properties of such bar and its effect on the host galaxy.

3 BAR FORMATION AND EVOLUTION

In this section, we first focus on the analysis of the build-up of the bar of ErisBH , by quantifying its strength and spatial extent across time. We then study the dynamical stability of the galactic disc,

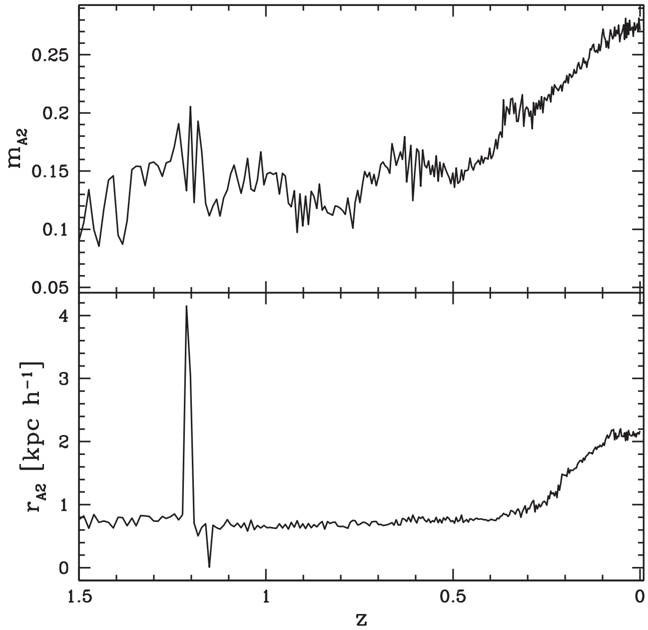

Figure 2. Evolution with redshift of m_{A2} (upper panel) and r_{A2} (lower panel). The early fluctuation at $z \approx 1.2$ is caused by the last minor merger experienced by the main galaxy. A clear transition towards constantly increasing values of m_{A2} and r_{A2} is observable at $z \lesssim 0.5$, associated with the growth of the galactic bar. A flattening in the m_{A2} and r_{A2} profiles is observable at low redshift $z \lesssim 0.1$ in correspondence of the boxy-peanut bulge formation, as discussed in the following.

to determine the conditions that led to the development of the bar. Finally, we study the emergence of the B/P morphology of the bulge and connect it to the growth of the bar.

3.1 Properties of the bar

In order to quantitatively assess the bar extent and strength, we perform a Fourier decomposition of the projected stellar density field $\Sigma_*(x; y)$ on the disc plane, and we calculate the *cumulative* A_2 amplitude, as introduced in Athanassoula & Misiriotis (2002) and already used in other works (e.g. Dubinski, Berentzen & Shlosman 2009; Fiacconi, Feldmann & Mayer 2015):

$$A_2(r) = \frac{1}{M} \sum_{j=1}^{N} m_j \, \mathrm{e}^{2\mathrm{i}\,\phi_j} \,, \tag{1}$$

where the summation is carried over the entire set of $N = N(r)$ star particles up to a distance r from the centre and M is the total mass within the same distance. Due to its definition, $A_2(r)$ increases up to the distance at which the $\Sigma(x; y)$ field structure exhibits a strong non-axisymmetric component and then gradually falls to zero. The radial position r_{A2} of the maximum value $m_{A2} = \max[A_2(r)]$ is used as an estimate of the bar radial extent. At the same time, the value of m_{A2} itself can be used as an estimate of the bar strength, as it measures the bar intensity with respect to the mean projected density field up to $r = r_{A2}$.

We calculate the $A_2(r)$ radial profile at each snapshot in order to trace the bar amplitude evolution as well as its radial extent evolution through time (Fig. 2). During the early stages of disc formation strong fluctuations in m_{A2} are due to ongoing minor merger events and/or the associated galaxy relaxation events. The last minor merger occurs at $z \sim 1.2$, after which the galaxy evolves practically in isolation.

From $z \sim 0.5$ and onward, the intensity of m_{A2} gradually increases with time and reaches a maximum of $m_{A2} \approx 0.27$ close to the end of the simulation. Results in Fig. 2 show that the bar radial extent also reaches its maximum value $r_{\max} \approx 2.2$ kpc at late simulation stages. The bar extent stabilizes about $r \approx 2.1$ kpc after $z \lesssim 0.1$, in correspondence with the growth of a central B/P bulge (see Section 3.3). The bar strength and the formation time we measure in ErisBH are consistent with previously published results obtained from both isolated and cosmological simulations (e.g. Kraljic, Bournaud & Martig 2012; Cole et al. 2014; Fiacconi, Feldmann & Mayer 2015; Polyachenko, Berczik & Just 2016), although we note that a large scatter is present in literature, particularly in the growth time (from $\lesssim$1 Gyr to $\gtrsim$3 Gyr for Milky Way-like galaxies).

3.2 Dynamical stability of the galactic disc

The absence of a central massive bulge makes the galaxy naturally unstable to the growth of a bar as soon as it settles in a dynamically cold rotationally supported structure. At $z < 1.5$, the disc's dynamical properties allow for the amplification of density perturbations through the *swing amplification effect* (see e.g. Binney & Tremaine 2008) which may easily promote the growth of a bar-like structure. The effectiveness of this process is linked to both the Toomre parameter Q and the swing amplification parameter X (see e.g. Toomre 1964; Goldreich & Tremaine 1978, 1979). For a differentially rotating stellar disc, the two parameters are defined as (see e.g. Binney & Tremaine 2008)

$$Q(R) = \frac{\sigma_r(R)\,\kappa(R)}{3.36\,G\,\Sigma(R)}; \quad X(R) = \frac{R\,\kappa^2(R)}{4\pi\,G\,\Sigma(R)}, \tag{2}$$

where $\sigma_r(R)$ is the radial velocity dispersion of the stars, $\kappa(R)$ is the epicyclic frequency, G is the gravitational constant and $\Sigma(R)$ is the star surface density. The Toomre parameter accounts for the disc stability to axisymmetric density perturbations: if $Q \le 1$, the disc is unstable. On the other hand, the swing amplification parameter X quantifies whether non-axisymmetric perturbations can grow. Two conditions must be simultaneously verified for the swing amplification to be effective: $Q \gtrsim 1$ so that the disc is stable but still strongly responsive to density perturbations, and $X \lesssim 3$ to prevent the density waves from being too tightly wound (see Binney & Tremaine 2008).

Fig. 3 shows the Q and X radial profiles calculated at four different times. As the two parameters are in the range $1 \lesssim Q \lesssim 2$ and $1 \lesssim X \lesssim 3$ (Fig. 3, red shaded areas in the left-hand panels), it is clear that an extended central region (i.e. up to $r \sim 3$ kpc) is prone to bar instability. For reference, the face-on view of the stellar surface density map of the galaxy is shown in the right-hand panels. The effect of the minor merger happening at $z \approx 1.2$ on stellar dynamics is observable both in the Q and X profiles (that show local peaks at the location of the satellite), as well as in the frequency plot, showing both the angular velocity Ω and the precessional frequency $\Gamma = \Omega - \kappa/2$, where κ is the epicyclic frequency. This merger imprints a degree of non-axisymmetry on the central stellar distribution. It is however unclear whether the merger-driven asymmetric structure is the seed of the stellar bar observable at lower redshifts or not. Because of the noisy evolution of the m_{A2} parameter at $z \gtrsim 0.5$, it is impossible to firmly assert that the bar starts growing already at $z \approx 0.8$ (1.5 Gyr after the completion of the merger), where a mildly increasing trend is discernible in the $m_{A2}(z)$ evolution (see Fig. 2, upper panel), or only at $z \approx 0.5$ (about 3.5 Gyr after the merger). For such reason, we refrain from commenting further on the trigger of the bar instability in this section. A discussion about possible

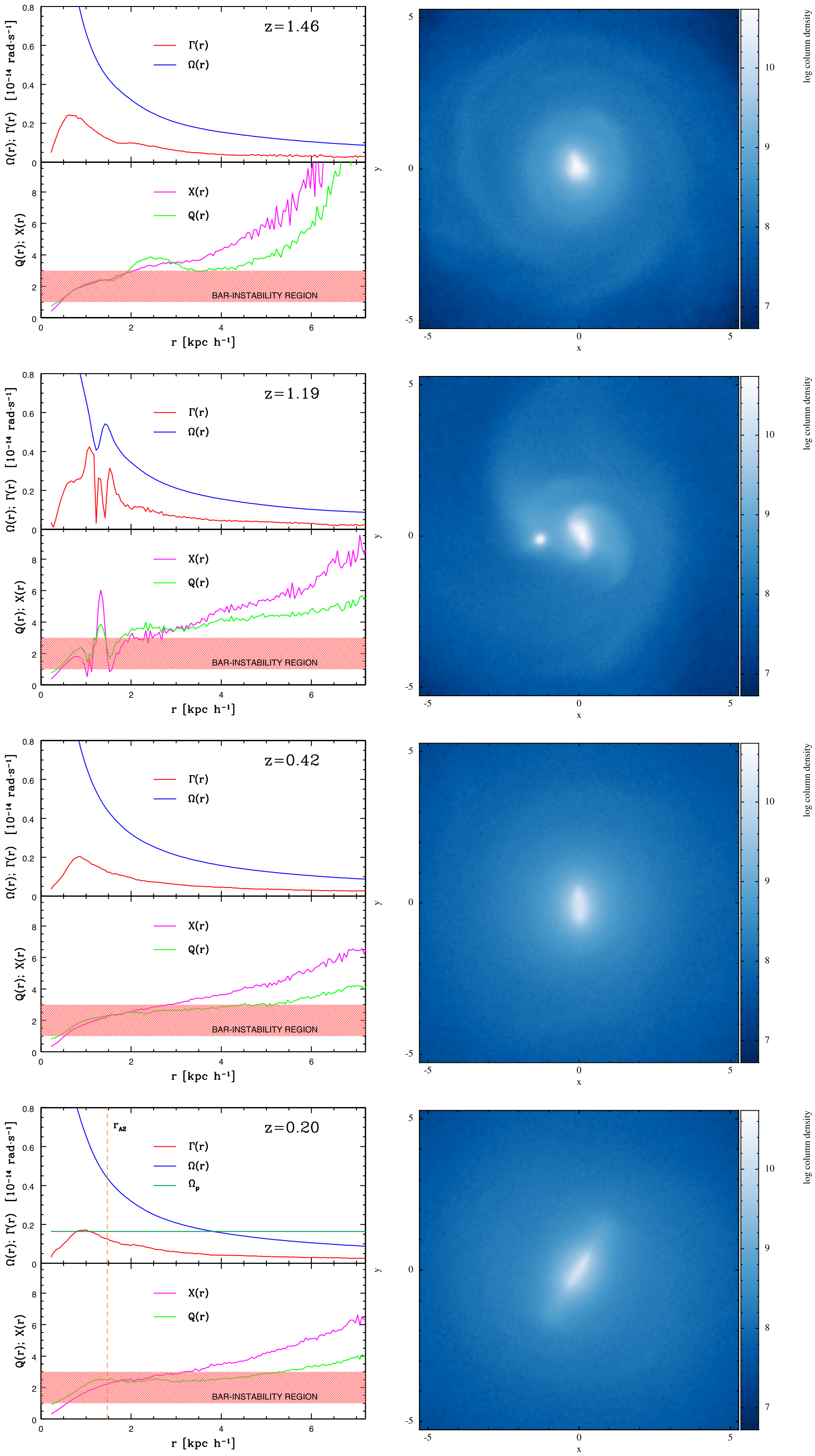

Figure 3. Dynamical and morphological structure of the main galaxies at different evolutionary stages. From top to bottom: before ($z = 1.46$), during ($z = 1.19$) and after ($z = 0.42$ and 0.20) the occurrence of the last minor merger. Left-hand panels: frequency plots (Ω and Γ, upper half) and Q and X stability parameters as a function of the radius. The red shaded area highlights the bar instability region ($1 \lesssim Q \lesssim 2$ and $1 \lesssim X \lesssim 3$) in each panel. The orange vertical dashed line in the bottom panel marks the bar extent, while the horizontal green line refers to the bar rotation frequency. Right-hand panels: face-on projection of the stellar density map at the corresponding redshifts. Colours encode the stellar surface density (in units of $M_{\odot}$ kpc^{-2}) on a logarithmic scale. The merging companion appears in the second panel from the top.

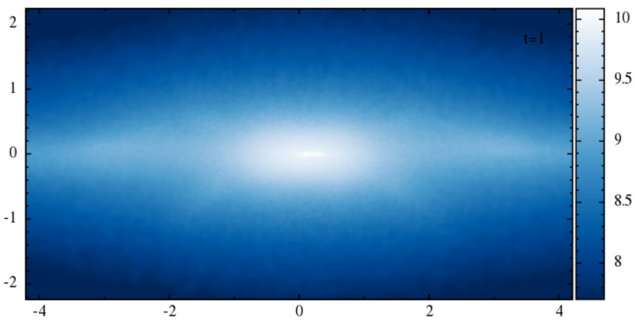

Figure 4. Edge-on view of the ErisBH last snapshot (redshift $z = 0$) in which the boxy-peanut shape is evident. The bar major axis is perpendicular to the line of sight to enhance the visibility of the boxy-peanut structure. Units are the same as in Figs 1 and 3.

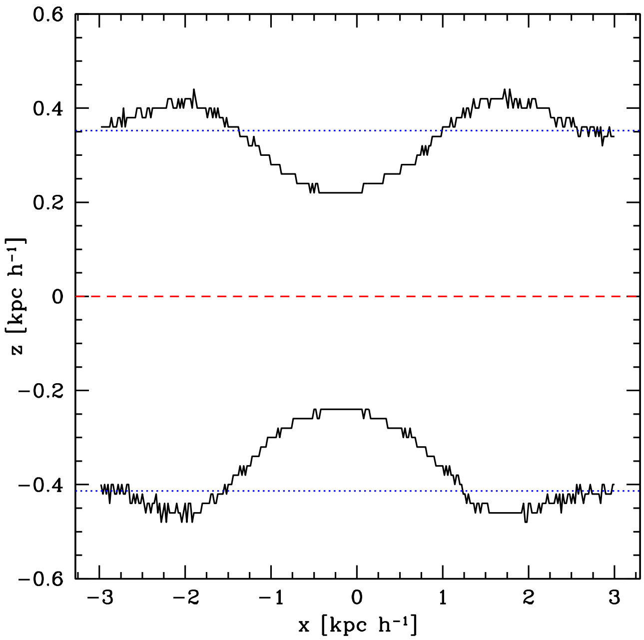

Figure 5. $|z|^+$ and $|z|^-$ profiles (black solid lines) with respect to the x coordinate, computed above and under the disc plane, respectively, at redshift $z = 0$. A double-horned feature is evident in both profiles, demonstrating the presence of a boxy-peanut structure in the central region of the galaxy (Iannuzi & Athanassoula 2015). The dashed horizontal red line marks the position of the galactic plane in the $(x; z)$ plane. The blue dotted lines are reference lines used to calculate the relative intensity of the peaks in the $|z|^+$ and $|z|^-$ profiles (see text).

future investigations designed to answer this particular question is presented in the conclusions.

The angular frequency ($\Omega_{\rm bar}$) and extent of the bar are shown in the lower-left panel of Fig. 3 (horizontal green and vertical red lines, respectively). The bar rotates with a frequency of $\approx$30 km s^{-1} kpc^{-1} at $z = 0$ which is similar to the frequency estimated for the Milky Way (Gerhard 2011) and approximately equal to the maximum of $\Gamma(R)$. This is somewhat expected, since perturbations with $\Omega_{\rm bar} \approx \max(\Gamma)$ are the fastest to grow, as demonstrated for the first time by Sanders (1977). The lack of a clear inner Lindblad resonance (ILR, defined by the equivalence $\Omega_{\rm bar} = \Gamma(R_{\rm ILR})$), of the kind of those observable in presence of a strong central concentration of matter (where Γ tends to diverge for small radii), maintains the elongated bar-like structure even at small (sub-kpc) radii (see Fig. 1). The consequences of the absence of a clear ILRs on the fate of the bar-perturbed gas will be discussed in the next section.

It is also evident that the bar does not extend out to its corotational radius ($R_{\rm cor}$ defined by the $\Omega_{\rm bar} = \Omega(R)$ equality), but stops at considerably smaller radii ($r_{\rm A2} \sim 0.5R_{\rm cor}$), in agreement with the results of previously published cosmological (e.g. Okamoto et al. 2015) as well as of idealized simulations which show tidally induced bars (e.g. Lokas et al. 2016). We stress however that the $r_{\rm A2}/R_{\rm cor}$ ratio we found is considerably smaller than that of most of the observed bars (e.g. Aguerri et al. 2015, and references therein), although some galaxies host bars whose $r_{\rm A2}/R_{\rm cor}$ ratios are consistent with the ones we find (Rautiainen, Salo & Laurikainen 2008). On a theoretical ground, small $r_{\rm A2}/R_{\rm cor}$ ratios have been predicted both for bars triggered by interactions (Miwa & Noguchi 1998) possibly like the one discussed here and for bars growing in galaxies with an initially low bulge-to-disc mass ratio (Combes & Elmegreen 1993), as it is the case of the ErisBH simulation.

3.3 The emergence of the B/P morphology of the bulge

As already commented, the bar stops growing when a B/P structure starts to form in the central region of the disc. The B/P feature can be easily pointed out by a qualitative edge-on view analysis of the ErisBH latest evolutionary stages (see Bonoli et al. 2016, and Fig. 4). To constrain the time evolution of the B/P structure, we perform a quantitative analysis on the edge-on projected density field at each snapshot. We first select the $(x; y)$ plane defined by the bar major axis and the direction perpendicular to the disc plane. On such a plane, we measure the $|z|^+(x)$ and $|z|^-(x)$ locations of the median value of the Σ_* above or below the disc plane as a function of the x position (as in Iannuzi & Athanassoula 2015). Fig. 5 shows an example of the $|z|^{\pm}(x)$ behaviour with respect to the x coordinate at redshift $z = 0$.

A double-horned shape is clearly visible in the $|z|^+(x)$ and $|z|^-(x)$ profiles. To study the growth in time of the B/P bulge, we first calculate two reference values z_0^+ and z_0^- on the $|z|^+$ and $|z|^-$ profiles, respectively, by averaging $|z|^+$ and $|z|^-$ in the intervals $x \in [-4; -3]$ and $x \in [3; 4]$ (outside the bar region, in the unperturbed disc, see the blue dotted lines in Fig. 5). This reference value is then used to measure the quantity

$$h = \max[\,|z|\,] - z_0 \tag{3}$$

on the four quadrants of the disc projection, and the average of the four values $h_{\rm m}$ is compared with $\sigma_r = \max[\sigma^+; \sigma^-]$ where σ^+ and σ^- are the standard deviations of the $|z|^+$ and $|z|^-$ profiles around the reference values z_0^+ and z_0^- in the outer disc.[2] If no double-horned feature is present in the $|z|^{\pm}(x)$ profiles, then $h_{\rm m}$ must be comparable to σ_r. The results of this analysis are shown in the upper panel of Fig. 6. It is evident that $h_{\rm m}(z)$ becomes consistently bigger than σ_r only after redshift $z \simeq 0.1$, i.e. the double-horned feature (and so the B/P structure in the bulge) develops at late evolutionary stages, when the bar is already strong, as shown by the $r_{\rm A2}$ evolution (shown for $z \lesssim 0.4$ in the lower panel of Fig. 6 for any easy comparison). In order to constrain the origin of the B/P bulge, we computed the parameter $B = (\sigma_z/\sigma_x)^2$ within the central 3 kpc of the disc, where σ_z and σ_x are the vertical and radial velocity dispersions measured on a slit along the bar major axis. As discussed in (Martinez-Valpuesta, Shlosman & Heller 2006, and references therein), $B \lesssim 0.3$ corresponds to a buckling unstable galactic nucleus. As expected, B decreases in

[2] We take the maximum between σ^+ and σ^- to be more conservative.

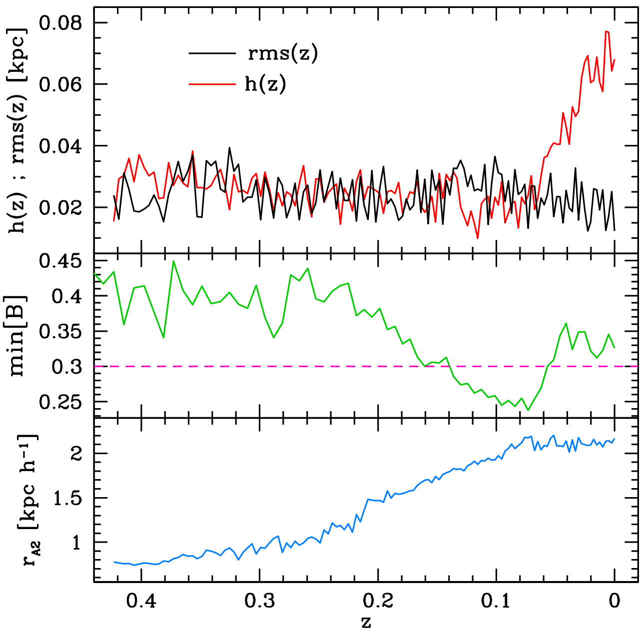

Figure 6. Upper panel: B/P strength as a function of redshift z. The red line refers to the relative height h of the $|z|(x)$ peak to a reference value z_0, while the error on the z_0 average σ_r is shown in black. Middle panel: minimum value of the parameter $B = (\sigma_z/\sigma_x)^2$ within the inner 3 kpc from the main galaxy centre, as a function of redshift. The bar is buckling unstable for $B \lesssim 0.3$. Lower panel: evolution of the bar length r_{A2} in the same redshift interval. Note that $h(z)$ becomes consistently bigger than σ_r towards the end of the simulation (upper panel), when the bar stops increasing its size and strength (lower panel).

time after the formation of the bar, because of the rise of σ_x, down to the buckling unstable regime. As soon as the B/P bulge forms, B rises again because of the increase in σ_z associated with the buckling event (see Fig. 6, middle panel). The buckling nature of the B/P structure is still observable in the asymmetric (with respect to the equatorial plane) mass distribution of the $z = 0$ disc (see Fig. 4). Fig. 6 shows that r_{A2} stops growing when the B/P structure forms and grows, consistently with the scenario of bars weakening proposed by e.g. Combes & Sanders (1981), Sellwood & Wilkinson (1993) and Kormendy (2013).

4 GAS RESPONSE TO THE BAR GROWTH AND CONSEQUENCES ON STAR FORMATION

In this section, we focus on the bar impact on its host evolution. In particular, we analyse the dynamical processes experienced by the gas in the region dominated by the bar and their consequences on star formation.

4.1 Gravitational torque and gas evolution

As the bar grows and gains strength, it starts exerting torques on the gas component of the galaxy, modifying completely its distribution in the central region. In Fig. 7, we show the surface density of the gas at four different epochs. The central region (approximately within 3 kpc from the centre) of the galaxy at $z = 0$ appears almost empty of gas, except for a density peak in the galactic nucleus on scales of the order of our spatial resolution ($\sim$100 pc). The quantitative evolution of the gas content in the galaxy centre is shown in Fig. 8, where we show the surface density profile of the gas at different times. In this case, we re-normalize the profiles in the unperturbed region of the galaxy ($4 \lesssim R \lesssim 10$ kpc). This allows us to emphasize the effect of the bar, averaging out the effects of cosmological gas accretion and star formation related gas consumption on large scales.

Figs 7 and 8 show the torquing effect that the growing bar has on to the gas. The gas within the bar extent is driven towards the centre of the galaxy,[3] and the majority of it is converted in stars (see below). Because of the absence of a clear ILR, the gas does not settle into a nuclear ring of star formation, but keeps on being torqued by the bar down to the very central region of the galaxy, where it forms a dense clump of $R \lesssim 200$ pc, whose internal structure we cannot resolve. The clump is surrounded by a gas-depleted region, as visible in the bottom-right panel of Fig. 7. To confirm this picture, we estimate the relevance of the torque that the stellar distribution exert on to the gas. Following Mundell & Shone (1999) and Emsellem et al. (2015), we calculate the strength of the torque using

$$Q_t(r) = \frac{\max\left[\frac{1}{r}\frac{\partial\phi(r;\theta)}{\partial\theta}\right]}{\left\langle\frac{\partial\phi(r;\theta)}{\partial r}\right\rangle_\theta} \quad (4)$$

which is the ratio between the maximum tangential force and the mean axisymmetric force at each radius r. The maximum value of Q_t can also be used to classify the bar strength, with $\max(Q_t) > 0.4$ corresponding to structures hosting strong bars (e.g. Buta, Laurikainen & Salo 2004; Buta et al. 2005). The torque profile at $z = 0$ is shown in Fig. 9. The maximum value of Q_t is $Q_t \approx 0.56$, confirming the strong bar nature of the central non-axisymmetric structure. More interestingly, the curve is peaked at very small radii close to our resolution limit, which explains the formation of a compact central gas overdensity and is consistent with the highly non-axisymmetric distribution of the stars at the smallest radii (see Fig. 1). The bar does persist until $z = 0$, thus most of the stellar mass in the inner 1–2 kpc remains associated with the bar rather than growing further the small pseudo-bulge. This is consistent with the notion that large central masses (of the order of a tenth of the total stellar disc) within a very compact size (well within one-tenth of the disc scalelength), are needed to destroy the bar (see e.g. Shen & Sellwood 2004), while here the central overdensity is modest (about 3 per cent of the total stellar mass within 300 pc), without any clear nuclear overdensity present.

We calculated the $Q_t(r)$ profiles at different times to sample the bar strength evolution with respect to time. We find that the maximum torque is always obtained near the galaxy centre (i.e. up to $r \simeq 250$ pc), confirming that the bar in ErisBH can be very effective in changing the gas angular momentum up to the very smallest radii and make it fall towards the centre. This means that the bar can efficiently feed the central region, providing the fuel necessary to ignite later evolutionary phenomena such as nuclear star formation (e.g. Kormendy 2013) and AGN activity (e.g. Combes 2001; Querejeta et al. 2016). In ErisBH , however, the accretion of matter on to the central MBH at low z is very modest (Bonoli et al. 2016). Most of the matter inflowing towards sub-kpc scales during the formation of the bar reaches densities large enough to be turned into stars (within a region of $\sim$600 pc), where nuclear star formation then becomes the dominant process, as we discuss below.

[3] We checked that the gas outflow from the central region is negligible by calculating the total mass in star and gas within the bar final extent ($r = 2.17$ kpc) with respect to redshift during the bar growth phase. We find that the total baryonic mass is conserved within $\sim$3 per cent of its value at $z \sim 0.45$ (before bar formation), thus excluding strong inflows/outflows of material.

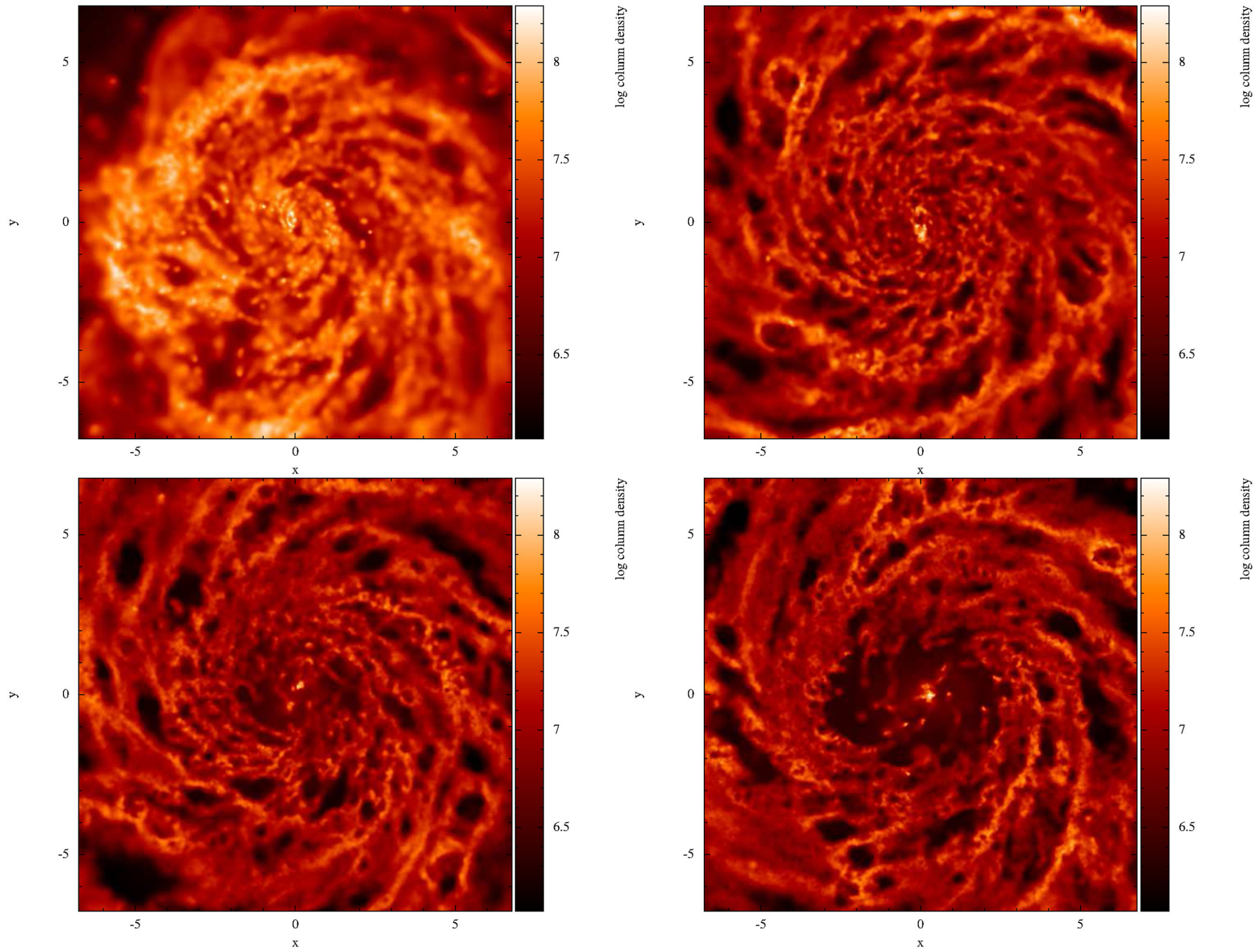

Figure 7. Map of the gas surface density at four different epochs, $z = 1.46$, 0.42, 0.20 and at the end of the simulation $z = 0$ (upper-left, upper-right, lower-left and lower-right panels, respectively). Units are the same as in Figs 1, 3 and 4 but we plot the gas surface density in a red colour scale.

4.2 Star formation and black hole accretion

The strong central gas inflows caused by the torques exerted by the growing bar, naturally lead to changes in the star formation and nuclear activity of the galaxy. Bonoli et al. (2016) already showed that the star formation rate and the black hole accretion rate increase after $z \sim 0.2$, which is when the bar is reaching maximum strength (see Fig. 2). Here, we further quantify the effect of the gas inflow on to the central star formation and nuclear activity. In Fig. 10 (upper panel), we show the radial distributions of young stars (with an age <0.6 Gyr, i.e. formed after $z \approx 0.05$) and those formed after the build-up of the bar structure at $z \approx 0.4$ (i.e. those with an age <4.5 Gyr). The ratio between these two quantities (bottom panel) clearly points out the presence of a recent star formation episode in the very central region of the galaxy (i.e. within ≈1 kpc).

A fraction of the inflowing gas gets accreted by the MBH. Fig. 11 (upper panel) shows the black hole accretion rate as a function of redshift from the last minor merger to $z = 0$. $\dot{M}_{\odot}$ is generally very low, fluctuating about a typical value of $2 \times 10^{-5}\,\mathrm{M}_{\odot}\,\mathrm{yr}^{-1}$ with the exception of some isolated spikes (see also Bonoli et al. 2016). This implies a modest growth of the black hole mass after $z \sim 1.2$, which undergoes a total increment of about ∼14 per cent of its final value (lower panel). A slight change in the accretion regime can be observed during the bar growth phase for $z \lesssim 0.3$. The accretion rate results, however, in a luminosity lower than ∼1 per cent of the MBH Eddington limit, assuming a radiative efficiency of $\eta = 0.1$. This further supports the picture in which the gas within the reach of the bar torques falls into the centre of the galaxy and is mainly consumed by bursts of nuclear star formation, while only a small fraction of it fuels the nuclear accretion process. As the gas infall proceeds all the way to the centre, it leaves behind a low gas-density region, a 'dead zone' visible at 500 pc–2 kpc in Fig. 8, within which star formation cannot be further sustained (Cheung et al. 2013; Fanali et al. 2015; Gavazzi et al. 2015b). The bar in ErisBH does not extend out to its corotational radius (see Fig. 3), i.e. its precession period is shorter than the orbital period of the outer gas. As a consequence, the bar exerts a positive torque on to the outer gas, preventing any further gas infall that could potentially replenish the dead zone.

On the contrary, the formation of new stars proceeds unimpeded outside the region affected by the bar. To further support this picture, Fig. 12 shows the face-on distribution of the youngest stars (i.e. with less than 35 Myr) at $z = 0$. The outer disc ($R \gtrsim 3$ kpc) is populated with large star formation regions, while only few young stars are present in the dead zone ($1 \lesssim R \lesssim 2$ kpc, i.e. the region between the two red circles). A nuclear ($\lesssim$1 kpc), elongated structure of young stars is hosted at the centre of the galaxy as a result of a recent star formation burst triggered by gas infall. A qualitative comparison

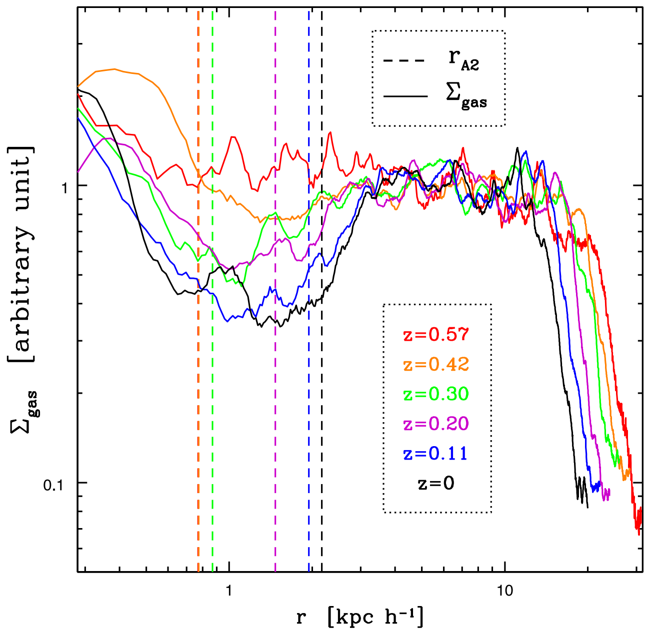

Figure 8. Gas surface density profile at different times. The dashed vertical lines show the bar extent at the different times. Note that the surface densities have been re-normalized to minimize the differences among the different profiles in the $4 \lesssim R \lesssim 10$ region.

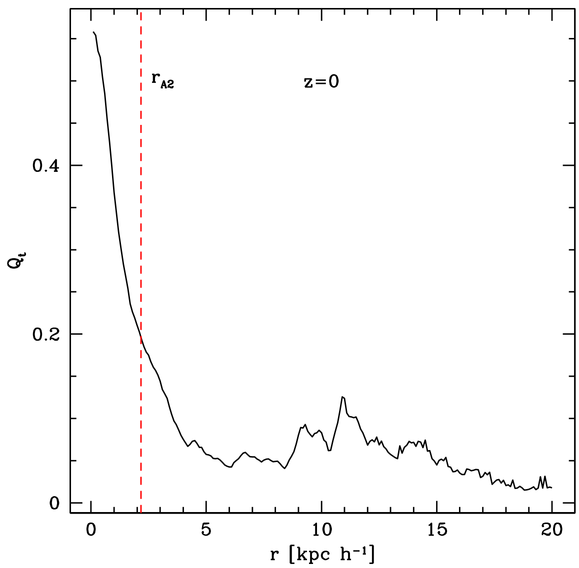

Figure 9. Radial profile of $Q_t(r)$ at $z = 0$ (black curve). The size of the bar (r_{A2}) at the same redshift is indicated by the red dashed line for reference. We see a prominent central peak ($Q_m = 0.56$ at $r \simeq 0.15$ kpc) and no relative maximum at $r \simeq r_{A2}$. It is remarkable that the profile monotonically decreases up to $r \simeq 4$ kpc from the centre. This shows that the bar non-axisymmetric structure is very coherent and the bar does not 'dissolve' into a spherical bulge at small radii. This implies also the possibility that the bar efficiently drives the gas inflow up to the very central region of the disc.

with the similar structure of NGC 1073 is shown in the right-hand panel of Fig. 12. The outer disc in NGC 1073 is mostly composed of star formation regions which host young stellar populations. On the contrary, a bar structure is evident in the galaxy centre where the almost exclusive presence of old and red stars is a prominent feature.

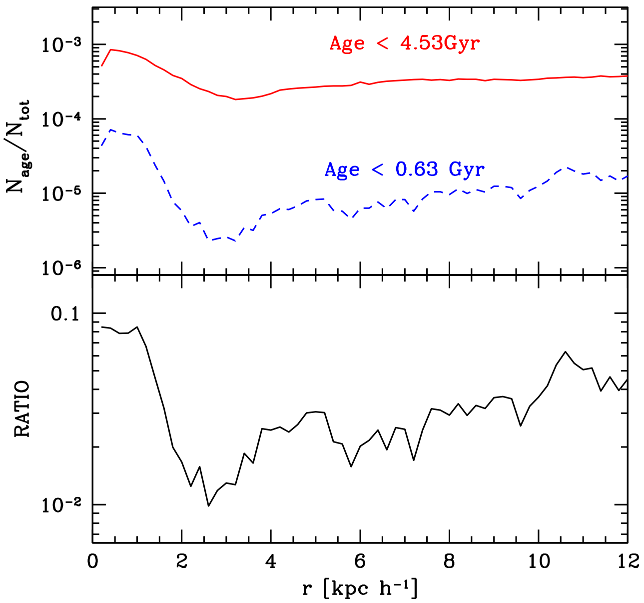

Figure 10. Upper panel: radial distribution at $z = 0$ of young stars formed after $z \approx 0.05$ (i.e. with an age <0.6 Gyr, blue dashed line) and stars formed after the bar build-up at $z \approx 0.4$ (with an age <4.5 Gyr, red solid line). The ratio of these two quantities (bottom panel) shows the signatures of a recent star formation episode (within ~1 kpc) which transformed into stars the gas torqued down by the bar gravitational effect. This produced a gas-poor 'dead zone' between $2 \lesssim r \lesssim 3$ kpc (see also Fig. 7 bottom-right panel) where a low number of young stars is present.

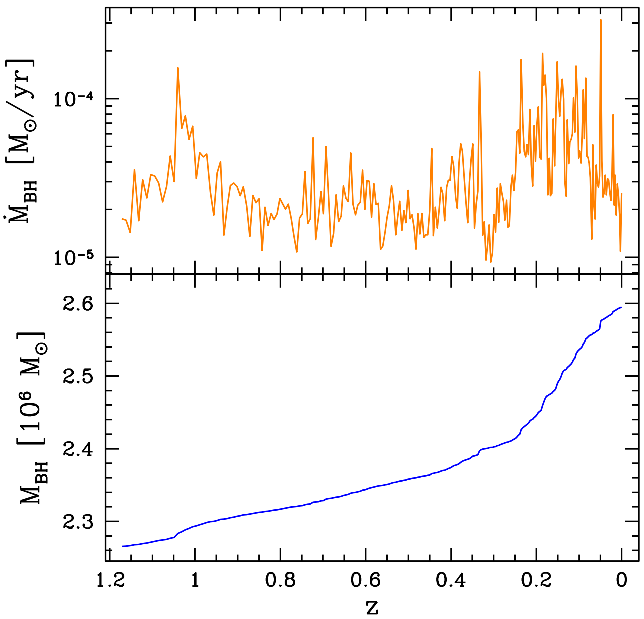

Figure 11. Accretion rate (upper panel) and mass evolution (lower panel) of the central black hole with respect to time. $\dot{M}_{\odot}$ is generally low confirming that the BH mass growth by gas accretion is very small after the last minor merger (about ~14 per cent of its final value). An increase in the MBH accretion rate is observable during the development of the bar structure; however, $\dot{M}_{\odot}$ remains modest even after $z \sim 0.3$.

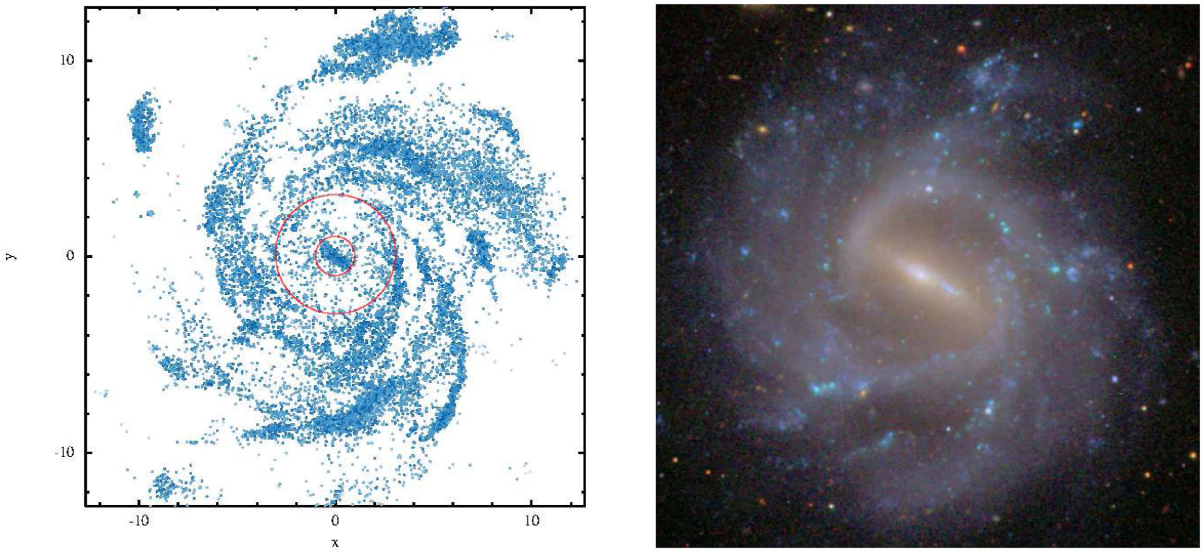

Figure 12. Left-hand panel: distribution at redshift $z = 0$ of the youngest stars, i.e. those with an age <35 Myr (formed at $z \approx 0.0026$, well after the bar build-up). The outer regions of the disc are populated with young stars, while a ‘dead region’ in which few young stars are present is highlighted by two red circles in the central region (i.e. at $1 \lesssim R \lesssim 2$ kpc from the centre). The nuclear region hosts a central bar-like distribution of young stars (at $R \lesssim 1$ kpc). Right-hand panel: the disc galaxy NGC 1073 is shown for a qualitative comparison. The outer regions of the NGC 1073 disc show star formation regions which host young stellar populations, while the inner regions exhibit a complex structure of older stars similar to that in ErisBH.

5 CONCLUSIONS

We analysed the high-resolution cosmological ErisBH run (Bonoli et al. 2016), which follows the evolution of a galaxy that, at $z = 0$, closely resembles an Sb/Sc galaxy with stellar mass and rotation velocity comparable to those of our Milky Way. At $z = 0$, the galaxy also features a strong nuclear ($R \approx 2$ kpc) bar which is able to influence: (i) the dynamics of the stellar disc, including the formation of a B/P bulge in its centre; (ii) the dynamics of the gas within the central 3 kpc, which falls towards the galactic centre triggering a short burst of star formation in the galactic nucleus (within ∼600 pc) as soon as the bar starts growing; (iii) the late star formation in the central ∼3 kpc. This is the consequence of the fast gas removal operated by the bar preventing any strong star formation episode after its formation.

The analysis of the torques operated by the bar supports the notion that the bar efficiently drives gas inflows down to the resolution limit (∼100 pc), due to the absence of any clear ILR at any $z \lesssim 0.4$. The absence of an intense star formation activity in the central regions of the disc at late times, as well as of strong AGN activity, is purely due to the absence of dense gas within the bar extent due to rapid consumption by star formation at the onset of bar formation ($z \simeq 0.4$). The lack of a clear observational correlation between AGN activity and the occurrence of bars in galaxies (see e.g. Ho, Filippenko & Sargent 1997; Mulchaey & Regan 1997; Hunt & Malkan 1999; Knapen, Shlosman & Peletier 2000; Laine et al. 2002; Lee et al. 2012b; Alonso, Coldwell & Lambas 2013; Cisternas et al. 2013; Cheung et al. 2015, for the different point of views) could be related to the prompt consumption of gas. If we assume that the results of ErisBH apply to the whole class of field disc galaxies in low-density environments, we argue that the strongest gas inflows and enhanced star formation happen at the onset of bar formation, when the detection of a bar is more difficult as the bar is shorter and less regular in shape. Instead, when the bar is stronger and well developed, hence easily detected through photometry or imaging, star formation has already ceased within a ‘dead zone’ in the galactic centre, making the occurrence of any nuclear activity less probable (see e.g. the discussion in Fanali et al. 2015).

Strong bars may arise at earlier times in more massive galaxies or galaxies living in dense environments, which evolve on shorter dynamical time-scales. Hence, we argue that bar formation can contribute to quenching and the formation of ‘red nuggets’ at $z > 1$, as also suggested by the results of the ARGO simulations which exhibit several example of early bar formation leading to increased central baryonic densities (Fiacconi, Feldmann & Mayer 2015). Bar-driven quenching should thus be seen as an alternative to mergers, disc fragmentation into massive clumps and AGN feedback, the main mechanisms explored in the literature over the last few years. Of course, bar-driven quenching is related to feedback mechanisms operating in the central region, as it seems to be the case in ErisBH where AGN feedback might be instrumental in creating favourable conditions for bar formation at later stages. Since bar formation requires a kinematically cold, thin disc to occur, it remains to be seen if this can be achieved by the latest generation of strong feedback models adopted in galaxy formation simulations.

It is interesting to note that such a strong bar is absent in the Eris run, which differs from ErisBH only because it does not feature any MBH accretion and feedback prescription. This would seem to be at odd with the limited gas accretion occurring on to the central MBH (Bonoli et al. 2016), that would imply a moderate effect of AGN feedback on to the host galaxy. However, at $z > 1$ there are transient near-Eddington accretion phases which ought to have an effect on the build-up of the central baryonic distribution. Indeed, at $z < 1$ ErisBH has a much flatter rotation curve near the centre as a result of the suppressed growth of the central baryonic density.

The actual trigger of bar growth is still to be pinpointed. The main galaxy in the ErisBH run becomes bar unstable at large redshift (see Fig. 3), but the bar structure forms only after the last minor merger episode. As discussed in Section 3, the properties of the bar do resemble those predicted for a tidally induced one. Whether the merger itself does provide the trigger for the instability to grow is unclear, as it is impossible to definitively constrain the time in between the merger and the actual onset of the bar growth. In order to test the possible tidal nature of the bar, we plan to run a set of simulations restarting the ErisBH run before the merger, removing the particles forming the satellite, and checking whether the bar grows regardless of the perturbation.

In conclusion, the present analysis of the ErisBH run has demonstrated that a bar resulting from the fully cosmological evolution of an isolated disc galaxy strongly affects its host, in particular by removing the gas from the region under its gravitational influence and producing a dead zone, on kpc scales, where star formation is quenched. This result provides further theoretical support to the recent claim by Gavazzi et al. (2015b) that bars can actually play a key role in the flattening observed at high masses in the star formation rate–stellar mass correlation (Whitaker et al. 2012, 2014; Magnelli et al. 2014; Gavazzi et al. 2015a; Ilbert et al. 2015; Lee et al. 2015; Schreiber et al. 2015, 2016).

ACKNOWLEDGEMENTS

We acknowledge Lia Athanassoula, Guido Consolandi, Victor de Battista, Luca Graziani and Giuseppe Gavazzi for the insightful comments and suggestions. Figs 1, 3 (right-hand panels), 4, 7 and 12 (left-hand panels) were produced using the SPLASH visualization tool for SPH data (Price 2007).

REFERENCES

Aguerri J. A. L. et al., 2015, A&A, 576, A102
Alonso M. S., Coldwell G., Lambas D. G., 2013, A&A, 549, A141
Athanassoula E., 1992, MNRAS, 259, 345
Athanassoula E., Misiriotis A., 2002, MNRAS, 330, 35
Athanassoula E., Lambert J. C., Dehnen W., 2005, MNRAS, 363, 496
Athanassoula E., Machado E. G., Rodionov S. A., 2013, MNRAS, 429, 1949
Bellovary J. M., Governato F., Quinn T. R., Wadsley J., Shen S., Volonteri M., 2010, ApJ, 721, L148
Berentzen I., Heller C. H., Shlosman I., Fricke K. J., 1998, MNRAS, 300, 49
Berentzen I., Shlosman I., Martinez-Valpuesta I., Heller C. H., 2007, ApJ, 666, 189
Binney J., Tremaine S., 2008, Galactic Dynamics, 2nd edn. Princeton Univ. Press, Princeton, NJ
Bird J. C., Kazantzidis S., Weinberg D. H., Guedes J., Callegari S., Mayer L., Madau P., 2013, ApJ, 773, 43
Bonoli S., Mayer L., Kazantzidis S., Madau P., Bellovary J., Governato F., 2016, MNRAS, 459, 2603
Buta R., Laurikainen E., Salo H., 2004, AJ, 127, 279
Buta R., Vasylyev S., Salo H., Laurikainen E., 2005, AJ, 130, 506
Cheung E. et al., 2013, ApJ, 779, 162
Cheung E. et al., 2015, MNRAS, 447, 506
Cisternas M. et al., 2013, ApJ, 776, 50
Cole D. R., Debattista V. P., Erwin P., Earp S. W. F., Roškar R., 2014, MNRAS, 445, 3352
Combes F., 2001, Advanced Lectures on the Starburst-AGN Connection. World Scientific Press, Singapore, p. 223
Combes F., Elmegreen B. G., 1993, A&A, 271, 391
Combes F., Sanders R. H., 1981, A&A, 96, 164
Consolandi G., Gavazzi G., Fumagalli M., Dotti M., Fossati M., 2016, A&A, 591, A38
Debattista V. P., Mayer L., Carollo M. C., Moore B., Wadsley J., Quinn T., 2006, ApJ, 645, 209
Dubinski J., Berentzen I., Shlosman I., 2009, ApJ, 697, 293
Emsellem E., Renaud F., Bournaud F., Elmegreen B., Combes F., Gabor J. M., 2015, MNRAS, 446, 2468
Fakhouri O., Chung-Pei M., Boylan-Kolchin M., 2010, MNRAS, 406, 2267
Fanali R., Dotti M., Fiacconi D., Haardt F., 2015, MNRAS, 454, 3641
Fiacconi D., Feldmann R., Mayer L., 2015, MNRAS, 446, 1957
Fisher D. B., Drory N., 2011, ApJ, 733, L47
Gabor J. M., Bournaud F., 2014, MNRAS, 441, 1615
Gavazzi G. et al., 2015a, A&A, 576, A16
Gavazzi G. et al., 2015b, A&A, 580, A116
Gerhard O., 2011, Mem. Soc. Astron. Ital. Suppl., 18, 185
Goldreich P., Tremaine S., 1978, ApJ, 222, 850
Goldreich P., Tremaine S., 1979, ApJ, 233, 857
Goz D., Monaco P., Murante G., Curir A., 2014, MNRAS, preprint (arXiv:1412.2883)
Guedes J., Callegari S., Madau P., Mayer L., 2011, ApJ, 742, 76
Guedes J., Mayer L., Carollo M. C., Madau P., 2013, ApJ, 772, 36
Hakobyan A. A. et al., 2016, MNRAS, 456, 2848
Ho L. C., Filippenko A. V., Sargent W. L. W., 1997, ApJ, 487, 591
Hunt L. K., Malkan M. A., 1999, ApJ, 516, 660
Iannuzzi F., Athanassoula E., 2015, MNRAS, 450, 2514
Ilbert O. et al., 2015, A&A, 579, A2
Jogee S., Scoville N., Kenney J. D. P., 2005, ApJ, 630, 837
Kim W.-T., Seo W.-Y., Kim Y., 2012, ApJ, 758, 14
Knapen J. H., Shlosman I., Peletier R. F., 2000, ApJ, 529, 93
Kormendy J., 2013, Secular Evolution of Galaxies. Cambridge Univ. Press, Cambridge, p. 1
Kraljic K., Bournaud F., Martig M., 2012, ApJ, 757, 60
Laine S., Shlosman I., Knapen J. H., Peletier R. F., 2002, ApJ, 567, 97
Laurikainen E., Salo H., Buta R., 2004, ApJ, 607, 103
Lee G.-H., Park C., Lee M. G., Choi Y.-Y., 2012a, ApJ, 745, 125
Lee G.-H., Woo J.-H., Lee M. G., Hwang H. S., Lee J. C., Sohn J., Lee J. H., 2012b, ApJ, 750, 141
Lee N. et al., 2015, ApJ, 801, 80
Lokas E. L., Ebrova I., del Pino A., Sybilska A., Athanassoula E., Semczuk M., Gajda G., Fouquet S., 2016, ApJ, 826, 227
Lütticke R., Dettman R. J., Pholen M., 2000, A&A, 362, 435
Magnelli B. et al., 2014, A&A, 561, A86
Martinet L., Friedli D., 1997, A&A, 323, 363
Martinez-Valpuesta I., Shlosman I., Heller C., 2006, ApJ, 637, 214
Mayer L., 2012, in Capuzzo-Dolcetta R., Limongi M., Tornambè A., eds, ASP Conf. Ser. Vol. 453, Advances in Computational Astrophysics: Methods, Tools, and Outcome. Astron. Soc. Pac., San Francisco, p. 289
Miwa T., Noguchi M., 1998, ApJ, 499, 149
Mulchaey J. S., Regan M. W., 1997, ApJ, 482, L135
Mundell C. G., Shone D. L., 1999, MNRAS, 304, 475
Nair P. B., Abraham R. G., 2010, ApJ, 714, L260
Okamoto T., Isoe M., Habe A., 2015, PASJ, 67, 63
Polyachenko E. V., Berczik P., Just A., 2016, MNRAS, 462, 3727
Price D. J., 2007, PASA, 24, 159
Querejeta M. et al., 2016, A&A, 588, A33
Rashkov V., Pillepich A., Deason A. J., Madau P., Rockosi C. M., Guedes J., Mayer L., 2013, ApJ, 773, L32
Rautiainen P., Salo H., Laurikainen E., 2008, MNRAS, 388, 1803
Regan M. W., Teuben P. J., 2004, ApJ, 600, 595
Roberts W. W., Jr, Huntley J. M., van Albada G. D., 1979, ApJ, 233, 67
Romano-Díaz E., Shlosman I., Heller C., Hoffman Y., 2008, ApJ, 687, L13
Roos O., Juneau S., Bournaud F., Gabor J. M., 2015, ApJ, 800, 19
Sanders R. H., 1977, ApJ, 217, 916
Sanders R. H., Huntley J. M., 1976, ApJ, 209, 53
Scannapieco C., Athanassoula E., 2012, MNRAS, 425, L10
Schreiber C. et al., 2015, A&A, 575, A74
Schreiber C., Elbaz D., Pannella M., Ciesla L., Wang T., Koekemoer A., Rafelski M., Daddi E., 2016, A&A, 589, A35
Sellwood J. A., 2014, Rev. Mod. Phys., 86, 1
Sellwood J. A., Moore E. M., 1999, ApJ, 510, 125
Sellwood J. A., Wilkinson A., 1993, Rep. Prog. Phys., 56, 173
Shen S., Sellwood J. A., 2004, BAAS, 36, 1551

Shen S., Madau P., Aguirre A., Guedes J., Mayer L., Wadsley J., 2012, ApJ, 760, 50
Shen S., Madau P., Guedes J., Mayer L., Prochaska J. X., Wadsley J., 2013, ApJ, 765, 89
Shlosman I., Frank J., Begelman M. C., 1989, Nature, 338, 45
Sokolowska A., Mayer L., Babul A., Madau P., Shen S., 2016, ApJ, 819, 1
Spergel D. N. et al., 2007, ApJ, 170, 377
Stinson G. S., Bailin J., Couchman H., Wadsley J., Shen S., Nickerson S., Brook C., Quinn T., 2010, MNRAS, 408, 812
Thacker R. J., MacMackin C., Wurster J., Hobbs A., 2014, MNRAS, 443, 1125
Toomre A., 1964, ApJ, 139, 1217
Villa-Vargas J., Shlosman I., Heller C., 2010, ApJ, 719, 1470
Wadsley J. W., Stadel J., Quinn T., 2003, New Astron., 9, 137
Whitaker K. E., van Dokkum P. G., Brammer G., Franx M., 2012, ApJ, 754, L29
Whitaker K. E. et al., 2014, ApJ, 795, 104

This paper has been typeset from a TEX/LATEX file prepared by the author.